JACS
JOURNAL OF THE AMERICAN CHEMICAL SOCIETY
Article
Cite This: J. Am. Chem. Soc. 2019, 141, 17207−17216
pubs.acs.org/JACS

Engineering Structural Dynamics of Zirconium Metal−Organic Frameworks Based on Natural C4 Linkers

Sujing Wang,[†,‡] Nertil Xhaferaj,[†] Mohammad Wahiduzzaman,[§] Kolade Oyekan,[∥] Xiao Li,[⊥] Kevin Wei,[∥] Bin Zheng,[§] Antoine Tissot,[†] Jérôme Marrot,[#] William Shepard,[▽] Charlotte Martineau-Corcos,[#,○] Yaroslav Filinchuk,[⊥] Kui Tan,[*,∥] Guillaume Maurin,[*,§] and Christian Serre[*,†]

[†]UMR 8004 CNRS, Ecole Normale Supérieure, Ecole Supérieure de Physique et de Chimie Industrielles de Paris, PSL Université, Institut des Matériaux Poreux de Paris, 75005 Paris, France

[‡]Hefei National Laboratory for Physical Sciences at the Microscale, University of Science and Technology of China, 230026 Hefei, China

[§]Institut Charles Gerhardt, Montpellier UMR 5253 CNRS ENSCM UM, Université Montpellier, Place Eugène Bataillon, 34095 Montpellier CEDEX 05, France

[∥]Department of Materials Science & Engineering, University of Texas at Dallas, Richardson, Texas 75080, United States

[⊥]Institute of Condensed Matter and Nanosciences, Université Catholique de Louvain, Place L. Pasteur 1, B-1348 Louvain-la-Neuve, Belgium

[#]Institut Lavoisier de Versailles, UMR 8180 CNRS, Université de Versailles Saint-Quentin-en-Yvelines, Université Paris-Saclay, 78035 Versailles, France

[▽]Synchrotron SOLEIL, L'Orme des Merisiers, Saint-Aubin, BP 48, 91192 Gif-Sur-Yvette, France

[○]CEMHTI, UPR 3079, CNRS, 45071 Orléans CEDEX 2, France

Supporting Information

ABSTRACT: Engineering the structural flexibility of metal−organic framework (MOF) materials for separation-related applications remains a great challenge. We present here a strategy of mixing rigid and soft linkers in a MOF structure to achieve tunable structural flexibility, as exemplified in a series of stable isostructural Zr-MOFs built with natural C4 linkers (fumaric acid, succinic acid, and malic acid). As shown by the differences in linker bond stretching and bending freedom, these MOFs display distinct responsive dynamics to external stimuli, namely, changes in temperature or guest molecule type. Comprehensive *in situ* characterizations reveal a clear correlation between linker character and MOF dynamic behavior, which leads to the discovery of a multivariate flexible MOF. It shows an optimal combination of both good working capacity and significantly enhanced selectivity for CO_2/N_2 separation. In principle, it provides a new avenue for potentially improving the ability of microporous MOFs to separate other gaseous and liquid mixtures.

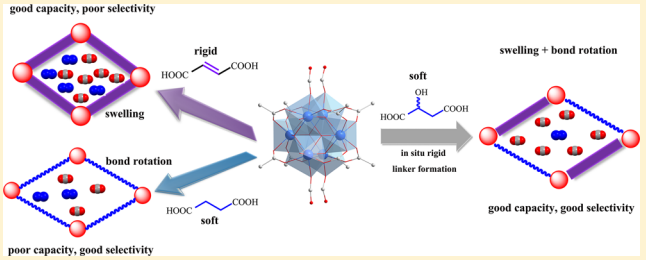

INTRODUCTION

Flexible metal−organic frameworks (MOFs) or porous coordination polymers (PCPs) represent a particular subgroup within the class of the hybrid materials, namely, the third generation compounds or soft porous crystals (SPCs).[1,2] In contrast to the first and second generations,[3−5] these materials display intriguing structural dynamics in response to external stimuli, such as guest molecule,[6−11] light,[12,13] temperature,[14−16] electrical field,[17] and pressure.[18−21] Consequently, numerous unique and unprecedented attributes have been discovered with regard to their applications in areas such as separation, sensors, catalysis, and biomedicine.[22−25] In this context, controlled inducement of the structural flexibility during MOF synthesis was regarded as an attractive strategy for targeting a given application. However, successful implementation remains a great challenge.

There are four major categories of flexibility identified for MOFs in the literature, including breathing, swelling, linker rotation, and subnetwork displacement.[26−28] In the case of breathing MOFs, such as the MIL-53 (Materials from Institute Lavoisier) series, the influence of phenylene ring rotation about its C−C axis to different extents are responsible for the notable changes in the unit cell.[14] A recent discovery of a

Received: July 22, 2019
Published: October 8, 2019

DOI: 10.1021/jacs.9b07816
J. Am. Chem. Soc. 2019, 141, 17207−17216

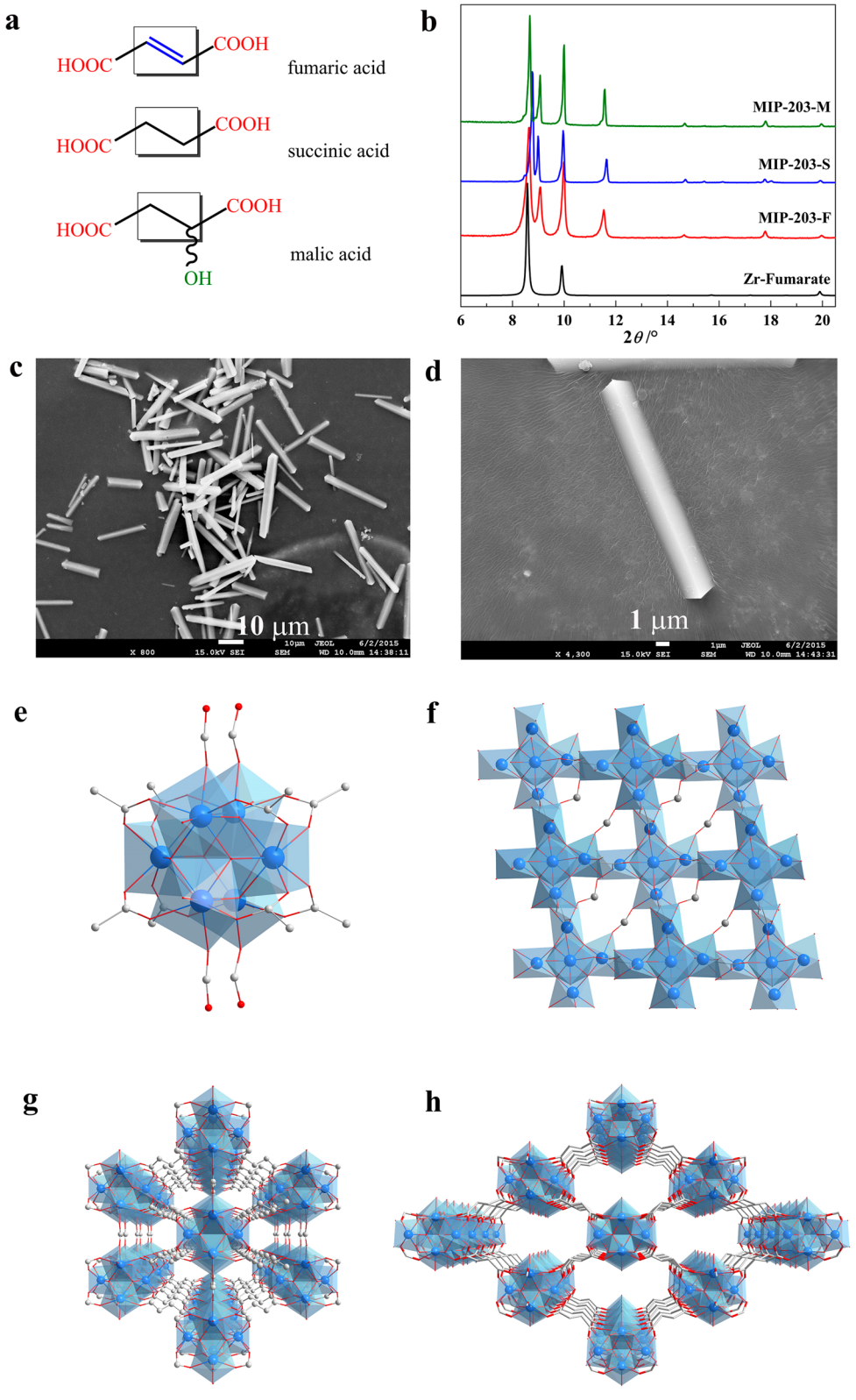

Figure 1. Structure details of MIP-203. (a) Chemical structures of the three naturally occurring dicarboxylic acids used in this work. (b) PXRD pattern comparison ($\lambda_{Cu} \approx 1.5406$ Å) between Zr-fumarate and MIP-203s. (c) and (d) Scanning electron microscopy (SEM) images of MIP-203-F with different magnifications. (e) The 10-connected $Zr_6(\mu_3\text{-}O)_4(\mu_3\text{-}OH)_4$ SBU showing eight linker carboxylates and two pairs of bridging formates in MIP-203-F. (f) and (g) Framework viewed along the *a*-axis and *b*-axis, respectively, clearly showing the bridging formates in MIP-203-F. (h) Framework viewed along the *c*-axis in MIP-203-F. Color scheme: Zr in blue, O in red and C in gray (hydrogen atoms are omitted for clarity).

breathing MOF displaying negative gas adsorption properties, namely, DUT-49 (Dresden University of Technology No. 49),[29] showed that metal node rotation could also lead to structural breathing, with noticeable bending of the biphenyl

DOI: 10.1021/jacs.9b07816
J. Am. Chem. Soc. 2019, 141, 17207−17216

moiety in the linker being detected as a result. For the swelling examples, such as MIL-88, metal node rotation is the sole driving force, with a very limited contribution to the overall change in the unit cell parameters from the linker.[30] Finally, linker rotation that does not induce significant changes in the unit cell has been observed in some "rigid" MOF structures such as ZIF-8 and MIL-140 that are built with rigid aromatic ligands.[28]

To the best of our knowledge, each flexible MOF reported has its unique combination of linker selection and inorganic building block. Consequently, the corresponding structural flexibility can only be tuned by the introduction of attached functional groups. The resulting linker bond distortion and bending are thus unrelated to the local freedom of bond stretching and rotation. Flexible aliphatic linkers with linear or cyclic alkane centers possess greater bond stretching and rotational freedom and are expected to favor the generation of dynamic structures. However, relevant studies in this field remain scarce.[23,31−33] Hence, it is very difficult to investigate the impact of the linkers' freedom of bond stretching and rotation on the softness of a given MOF type when the rigid and flexible linker pair is unable to generate isostructural MOFs. In this regard, it would be of great interest to engineer the structural flexibility in a series of isostructural MOFs using the same inorganic building block and linkers of similar molecular size and configuration but with different degrees of structural freedom (in both bond stretching and rotation), in order to understand how the local and structural dynamics of the architectures are governed by the linker characters.

To achieve this goal, the expected MOF candidates should fulfill the following requirements: (1) isostructural analogues built with linkers of different degrees of freedom; (2) an inorganic building block exhibiting a possible plane of symmetry, allowing the cooperative movements of various bonds involved; (3) frameworks featuring an accessible porosity to certain stimuli that can easily be detected, analyzed, and compared; (4) compounds being robust to avoid any structural deterioration.

Herein, we present a series of isostructural MOFs based on 10-connected Zr_6 clusters and natural C4 carboxylate linkers with linear aliphatic chains, denoted as MIP-203-F, MIP-203-S, and MIP-203-M (MIP stands for the Materials of the Institute of Porous Materials from Paris, F for fumaric acid, S for succinic acid, and M for malic acid), designed to engineer structural flexibility based on the nature and degree of freedom of the linker. While MIP-203-F is constructed using double-bonded fumarate and MIP-203-S is built with single-bonded succinate, MIP-203-M contains a sparse framework displaying multivariate flexibility,[28] with two-thirds fumarate and one-third malate as linkers resulting from a particular *in situ* dehydration reaction of malic acid into fumaric acid. The response of these MOFs' structural dynamics to external stimuli, namely, thermal activation and guest molecule inclusion, has been characterized in detail in order to investigate the possible correlation between linker degree of freedom and MOF dynamics. MIP-203-F shows noticeably more swelling flexibility compared to MIP-203-S, due to the differences between rigid fumarate and flexible succinate. The effective combination of two types of flexibility in MIP-203-M, namely, swelling and bond distortion or bending, results in the best selectivity for CO_2/N_2 separation. This suggests a new avenue for improving the ability of microporous MOFs to facilitate the separation of a wide range of vapors or gaseous mixtures. Moreover, these Zr-MOFs feature good chemical stability, cheap and biocompatible natural linkers, and green, scalable synthetic routines, all of which make them promising candidates for future practical applications.

RESULTS AND DISCUSSION

Among the reported inorganic building blocks having a possible symmetry plane, the Zr_6 cluster is one of the best options owing to its high connectivity and chemical stability, natural abundance, and low toxicity. The $Zr_6O_4(OH)_4$ cluster is one of the most common secondary building units (SBUs) reported in the literature.[34,35] The varying node connectivity, including the 12, 10, 8, 6, and 4-connected Zr_6 oxocluster in MOFs, allows a high degree of tunability of the corresponding MOFs structures, which provides a better opportunity to achieve a flexible crystal architecture. The 12-connected Zr_6 cluster has the densest connection environment and, thus, less freedom and space for configuration rearrangement. Alternatively, reducing the connectivity of the Zr_6 cluster could be more favorable to introduce structural flexibility.[11] In view of these factors, Zr-MOFs with low connectivity SBUs were preferentially considered as the model compounds.

Judicious use of flexible linkers has already been demonstrated to be an efficient strategy for generating soft MOFs structures when the inorganic SBUs are rigid.[23,28] Among the reported flexible linkers, naturally occurring compounds are of particular interest, as they are biocompatible and thus efficiently reduce the toxicity of the resulting MOFs. In the limited cases of reported Zr-MOFs composed of natural acids,[34] fumaric acid and its derivatives are dominant despite the fact that they all share the 12-fold connectivity, which highlights the controllable crystallization of Zr-fumarate type frameworks,[36−39] as well as the rigid structural character of fumaric acid, which is the same as evidenced in other MOFs.[24,25,40] On the contrary, succinic acid, which behaves as a soft molecular spring as seen in Co-MOFs,[41,42] has molecular lengths and configurations similar to those of fumaric acid. The most noticeable difference between succinic acid and the double-bonded fumaric acid is the former's single-bonded carbon skeleton, which usually exhibits greater freedom of stretching and rotation. In view of these features, fumaric acid and succinic acid, as the simplest pair of rigid and flexible natural carboxylic linkers, were selected for their typicality and suitability for the aforementioned target. Additionally, malic acid, a succinic acid derivative with a hydroxyl group on the alkane chain, was also used to check the impact of the side functional group.

Fumaric acid (Figure 1a) was used first to react with $ZrCl_4$ as the model reaction. Formic acid has been proven to be a modulating agent to generate the 12-connected structure with improved crystallinity in the preparation of Zr-fumarate (as known as MOF-801).[43] We expected that the increase in the amount of formic acid in the reaction solution could decrease the connectivity of the Zr_6 cluster, leading to less rigid structures with lower structural symmetry. Pure formic acid was used as the solvent in this case since it has been shown to be an efficient solvent for preparing group IV metal-based MOFs.[38,44] As expected, instead of forming the well-known Zr-fumarate structure MIP-203-F, a new phase with lower structural symmetry was obtained (Figure 1b). When succinic acid was used under the same reaction conditions, a clear solution was observed without any solid product, possibly due to the much greater solubility of succinic acid in formic acid.

DOI: 10.1021/jacs.9b07816
J. Am. Chem. Soc. 2019, 141, 17207−17216

After the reactant concentrations and the ratio between $ZrCl_4$ and succinic acid were optimized, the expected isostructural product was successfully obtained. The synthesis of MIP-203-M could be achieved by adjusting the reactant ratio under similar conditions (see SI for detail).

The crystal structure model of MIP-203 was initially determined on MIP-203-S using a dual computational and experimental approach, developed on the principle of automated assembly of structure building unit (AASBU) theory, that combines high-resolution powder X-ray diffraction data and our in-house crystal structure prediction software.[45] Afterward, needle-like single crystals of MIP-203-F with a homogeneous size and shape distribution (Figure 1c,d) were subjected to the synchrotron diffraction single-crystal data collection with a microfocused X-rays on the Proxima 2A beamline (Synchrotron SOLEIL, France),[46] in order to experimentally confirm the major framework connectivity of the simulated structure model.

Since the three MIP-203 compounds are isostructural, MIP-203-F was used as an example to detail their structural features. It was found that MIP-203-F, $Zr_6(\mu_3\text{-}O)_4(\mu_3\text{-}OH)_4(fumarate)_4(formate)_2(OH)_2(H_2O)_2$, crystallizes in an orthorhombic *Immm* space group with unit cell parameters of a = 10.000(2) Å, b = 11.940(2) Å, c = 19.829(11) Å, and V = 2367.6(15) Å^3. The Zr_6 SBUs (Figure 1e) were interconnected with one another by both fumarate and formate linkers, resulting in the final three-dimensional (3D) framework. It is, to the best of our knowledge, the first time that a Zr_6 SBU with mixed linkage from two highly dissimilar linkers in terms of shape, configuration, and connectivity has been generated using direct synthesis for Zr-MOFs. Formate serves as the auxiliary ligand connecting the adjacent SBUs along the c-axis. However, its presence blocks the window of the pores along the a-axis (Figure 1f). When the structure is viewed along the b-axis (Figure 1g), formates are shown to occupy the middle of the large rhombic channels, dividing them into two 4 Å sized triangular channels, which is also observed in the case of UiO-66(Zr) type structures.[47] Due to the presence of the terminal OH^- and H_2O pairs in the SBU, rhombic channels run along the c-axis without any blocking species (Figure 1h). Simulation results indicate that both MIP-203-F and MIP-203-S possess almost identical pore volumes (0.27 and 0.25 cm^3 g^{-1} for MIP-203-F and -S, respectively) and pore sizes estimated from the PSD plots (largest pore diameters ∼5 Å, Figure S3). However, due to the difference between C—C single and C═C double bonds, fumaric and succinic acids show slightly different conformations (see Figures S4−S6), resulting in the pore shape and dimension of these compounds varying to some extent (Figure S3).

An *in situ* dehydration reaction occurred when malic acid was introduced to the synthesis of MIP-203-M, leading to the transformation of two-thirds malic acid into fumaric acid. MIP-203-M can therefore be considered the corresponding product of replacing one-third fumarate in MIP-203-F by malate, as evidenced by solid-state NMR data (Figure S7). The coexistence of fumarate and malate in MIP-203-M makes it an unusual example of the MOF compound that shows multivariate flexibility through direct synthesis.

Thermal and chemical stability tests of MIP-203s were carried out before investigating and comparing the response to different external stimuli of the MIP-203s (Figures S10 and S11). Afterward, the influence of the thermal activation of the as-synthesized samples was first studied. As shown in Figure 2a, the as-synthesized MIP-203-F sample displays four PXRD peaks at low angle, i.e., 8.46, 8.94, 9.86, and 11.36° corresponding to the (011), (002), (101), and (110) Bragg peaks, respectively. After activating the sample at 100 °C under vacuum, the distinct shifts to higher angle domains for the

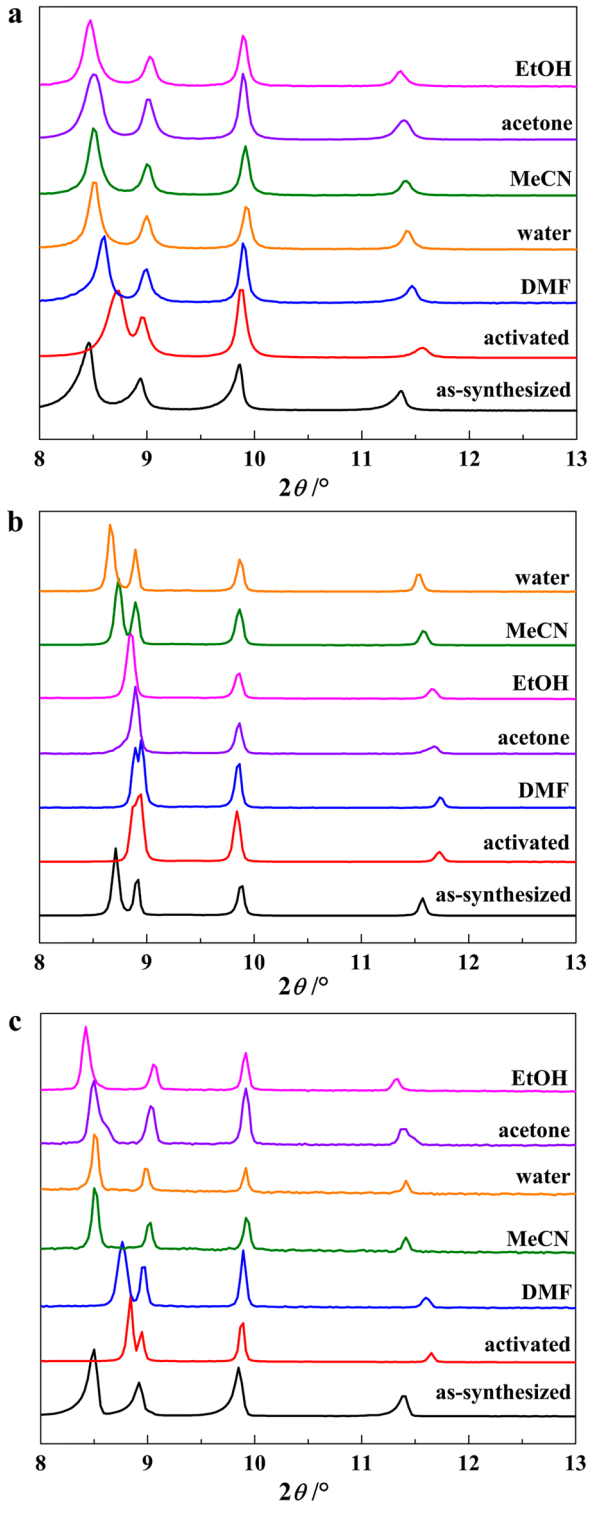

Figure 2. Structural response at room temperature of MIP-203s to liquid external stimuli (PXRD, $\lambda_{Cu} \approx 1.5406$ Å). (a) MIP-203-F in different solvents. (b) MIP-203-S in different solvents. (c) MIP-203-M in different solvents.

DOI: 10.1021/jacs.9b07816
J. Am. Chem. Soc. 2019, 141, 17207−17216

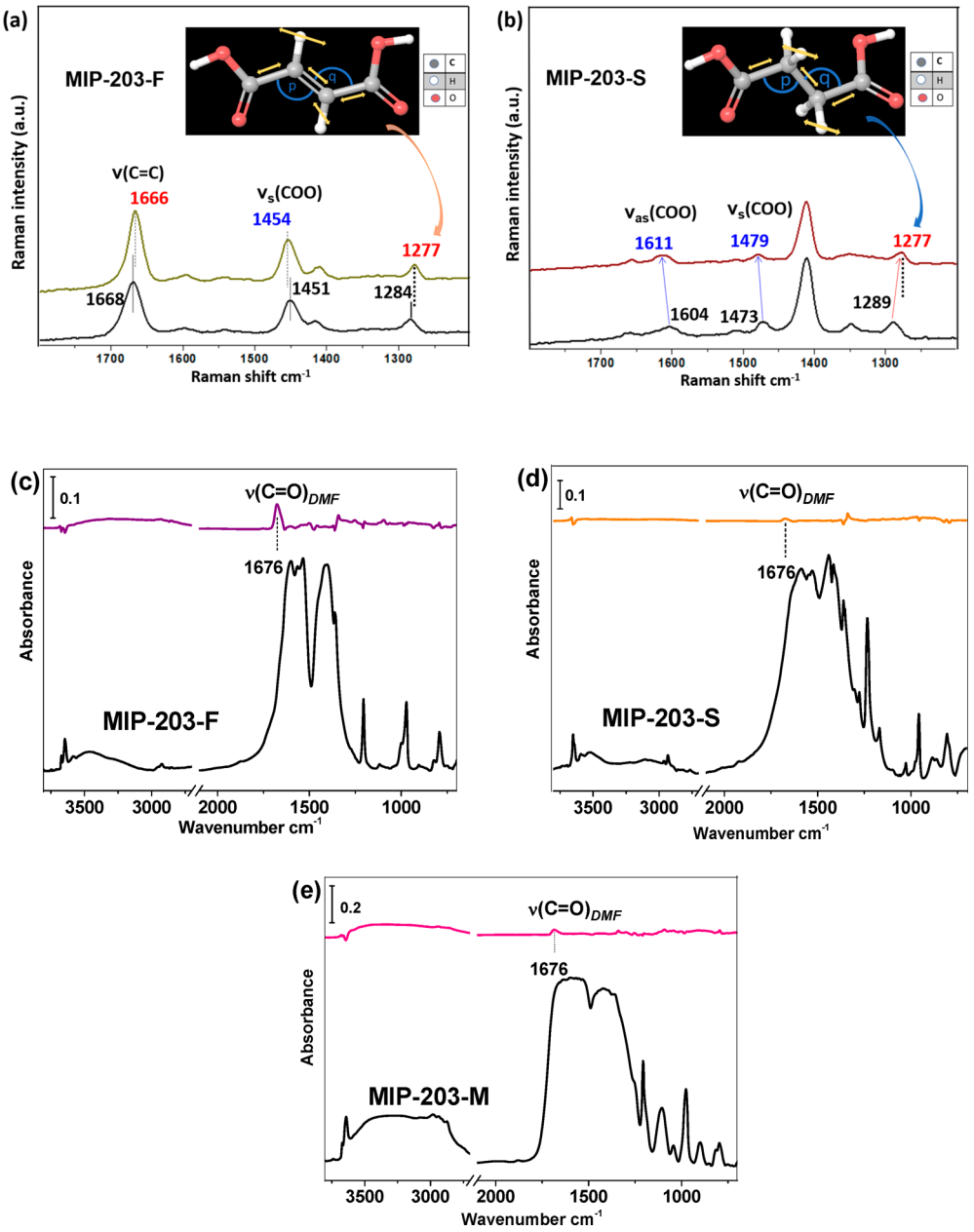

Figure 3. Raman spectra of MIP-203-F (a) and MIP-203-S (b) in as-synthesized (top lines) and dried (bottom lines) forms upon *in situ* activation. The spectra are collected at room temperature. *In situ* IR spectra of adsorbed DMF in MIP-203-F (c), MIP-203-S (d), and MIP-203-M (e), referenced to the activated MOFs (bottom black lines) under vacuum.

peaks at 8.73 and 11.56° were observed; this could be ascribed to the notable decrease of the *b* unit-cell parameter in the activated sample (11.856 Å) in comparison with that of the as-synthesized one (12.246 Å). The larger change in *b* compared to *a* and *c* could be explained by the weaker connection along the *b*-axis in the crystal structure, while the presence of bridging formates undoubtedly enhances the overall rigidity of the *a*−*c* plane. Similar observation was noticed between the as-synthesized and activated samples of both MIP-203-S and MIP-203-M (Figure 2b,c). The cell volume of the activated samples decreased by 57.6 $Å^3$/2.4%, 73.9 $Å^3$/3.1%, and 80.4 $Å^3$/3.4% for MIP-203-F, -M, and -S, respectively, in comparison with those of the as-synthesized ones, suggesting their similar structural contraction abilities upon thermal stimuli (Tables S2, S3, and S4).

In situ Raman spectroscopy was further employed to monitor the changes occurring in specific bonds in the MOF structure upon activation. Parts a and b of Figure 3 present the most pronounced changes in the range 1800−1200 cm^{-1} caused by *in situ* activation of the sample at 100 °C (see full spectra in Figure S9). In comparison to the as-synthesized MIP-203-S, the peak centers of the carboxylate stretching bands $\nu_{as}(COO)$ and $\nu_{s}(COO)$ in the activated sample are blue-shifted by 7 and 6 cm^{-1}, respectively, indicative of the bond hardening due to structural contraction upon removal of the solvents. The corresponding $\nu_{s}(COO)$ change in MIP-203-F sample is only 3 cm^{-1} and the $\nu_{as}(COO)$ peak intensity is too weak to be addressed, which evidences a much less pronounced bond change compared to that of MIP-203-S. Furthermore, a band at 1289 cm^{-1} for activated MIP-203-S with a 11 cm^{-1} red shift compared to the as-synthesized one,

DOI: 10.1021/jacs.9b07816
J. Am. Chem. Soc. 2019, 141, 17207−17216

was assigned to the vibration mode that involves $-CH_2$ wagging coupled with C—C—C—C stretching (see the attached videos 1 and 2). On the contrary, only a 7 cm^{-1} difference (1277 to 1284 cm^{-1}) for the −CH wagging in C—C═C—C was detected for MIP-203-F before and after the thermal activation. This mode has been shown to be very sensitive to changes in the bond angle of the carbon chain.[48] As shown in Figure 3a,b by DFT calculation, when the angles p and q (p and q are bond angles of the C4 skeleton of the linker) are decreased by ∼2 and ∼4°, respectively, for fumaric acid and ∼5 and ∼5° for succinic acid, its frequency shifts downward by ∼10 and ∼15 cm^{-1} in fumaric acid and succinic acid, respectively. The trend of these shifts is in good agreement with the experimentally observed values. It also matches well the similar observation reported on other flexible MOFs.[48] The above results point out the origin of different structural contraction responses arising from the distortion or bending of the C—C═C—C and C—C—C—C chains for MIP-203-F and MIP-203-S, respectively. This indicates that the local stretching and vibration freedoms of the succinate single-bonded skeleton are more pronounced than those of the fumarate double-bonded one. This observation is also supported by a much smoother evolution of the DFT-calculated potential energy for the succinate-cluster model vs the fumarate one when one varies the dihedral angle of the organic linker from its minimum-energy value, suggesting a higher ability of distortion for the succinate linker (Figures S4−S6). The spectra of MIP-203-M are dominated by a strong fluorescence signal and thus are not presented here.

The structural responses of MIP-203s to exposure to liquid guest molecules were then investigated. Activated samples of these three MOFs were exposed to diverse solvents and high-resolution PXRD patterns were collected with wet samples sealed in capillaries. The corresponding results are shown in Figure 2, and the indexing summary is listed in Tables S2−S4.

When the dried MIP-203-F sample was exposed to different solvents, the MOF framework allowed all the solvent molecules to enter the pore. The structural variation shows slight dependence on the molecular sizes and shapes of the solvent guest. A continuous increase of their unit cells along the b-axis was observed following the order of N,N-dimethylformamide (DMF) < water < acetonitrile < acetone < ethanol (Table S2), indicating that the MIP-203-F presents a tunable structural swelling property.

In contrast, the dried MIP-203-S sample displayed strict compatibility with solvent molecules according to their sizes and shapes (Figure 2b). Solvent molecules with larger sizes or branched shapes, such as DMF, acetone, and ethanol, could hardly enter the dynamic pore of MIP-203-S, evidenced by the comparatively minimal changes in its PXRD pattern. It is possibly that the single-bonded aliphatic linkers tend to stay in a closely packed configuration when the pores are in a guest-free form. For the loading of accessible solvent molecules, the MOF structure expands dramatically along with a notable increase of the b unit cell parameter. Correspondingly, their PXRD patterns show marked changes compared to that of the activated sample and are similar to that of the as-synthesized one. Therefore, this selective inclusion of solvent molecules based on their sizes and shapes reflects the effect of the local bond distortion or bending generated from the succinate aliphatic chain rather than the framework structural swelling.

In the case of MIP-203-M, the response to the loading of solvent molecules exhibits a combined effect observed in MIP-203-F and MIP-203-S. As shown in Figure 2c, solvent molecules with large sizes and branches, such as DMF, have a lesser effect on the MOF structure expansion, mainly due to the local bond distortion or bending and steric hindrance of the malate linker. Smaller solvent molecules could diffuse more easily into the MOF pore. In other words, a good structural swelling flexibility of the framework associated with an appropriate local bond distortion or bending toward guest molecules has been achieved in MIP-203-M.

In situ IR spectroscopy was employed to probe the interactions between the guest solvent molecules and the framework. DMF was chosen as the representative solvent to study its adsorption in the selected MOFs, due to the structural responses of these MOFs to DMF solvent showing significant variation (Figure 2). A vapor pressure of 4 Torr of DMF was introduced into the activated MOFs samples for ∼5 min to reach the adsorption equilibrium with the adsorbed DMF; this was characterized by a carbonyl stretching band ν(C═O) at 1676 cm^{-1}, shifted by 39 cm^{-1} from the center of the gas phase band (Figure 3 and Figure S8). A comparison of the intensities of the ν(C═O) band at 1676 cm^{-1} in the IR spectra of Figure 3 indicates that the uptakes of adsorbed DMF in these three samples exhibits the following trend: MIP-203-F > MIP-203-M > MIP-203-S.

It is well-documented in the literature that flexible MOFs show a great promise in dynamic separation of practical gases mixtures,[35,49−51] such as carbon dioxide over nitrogen in the postcombustion process. Considering the distinct response of MIP-203s to thermal activation and the adsorption of liquid guest molecules shown above, we speculated that similar behaviors could be observed when exposed to gas phase guest molecules. Single-component gas sorption measurements of N_2 and CO_2 under various conditions were performed. Nitrogen adsorption data collected at 77 K show clearly that the pores in MIP-203-F are accessible to N_2 molecules, displaying a typical type I adsorption isotherm associated with a Brunauer−Emmett−Teller (BET) area of 430 $m^2\ g^{-1}$ and a total pore volume of 0.24 $cm^3\ g^{-1}$. In a sharp contrast, MIP-203-S did not show any accessible porosity to N_2 at 77 K (Figure 4a). It is likely that the soft single-bonded C4 skeleton of succinic acid can distort more than fumaric acid with a C═C double bond. After thermal activation under vacuum to remove the guest molecules, MIP-203-S tends to stay in a closely packed form so that it is not accessible to nitrogen. When the adsorption temperature was increased to 273 K, the thermodynamic motions of single-bonded aliphatic chain of succinate resulted in a slight increase of N_2 uptake (Figure S12). The much higher uptake for MIP-203-F at 273 K suggests its more pronounced swelling ability toward nitrogen sorption stimuli or larger pore opening in its activated form. In the case of MIP-203-M, it shows a BET area of 380 $m^2\ g^{-1}$ and pore volume of 0.21 $cm^3\ g^{-1}$ comparable to those of MIP-203-F, indicating the beneficial effect of the fumarate content. A notable reduction of N_2 uptake was, however, observed at 273 K in comparison with that of MIP-203-F, showing the critical role of the soft malate content.

When the probe molecule was switched to the smaller sized CO_2, the influence of linker softness on the structural dynamics is much less pronounced. MIP-203-S exhibits half the uptake of CO_2 compared to MIP-203-F over almost the entire pressure range at 273 K (Figure S13). However, a significant decrease in CO_2 uptake was observed for MIP-203-S when the adsorption temperature was increased to 298 K. The uptake at 1 bar drops

DOI: 10.1021/jacs.9b07816
J. Am. Chem. Soc. 2019, 141, 17207−17216

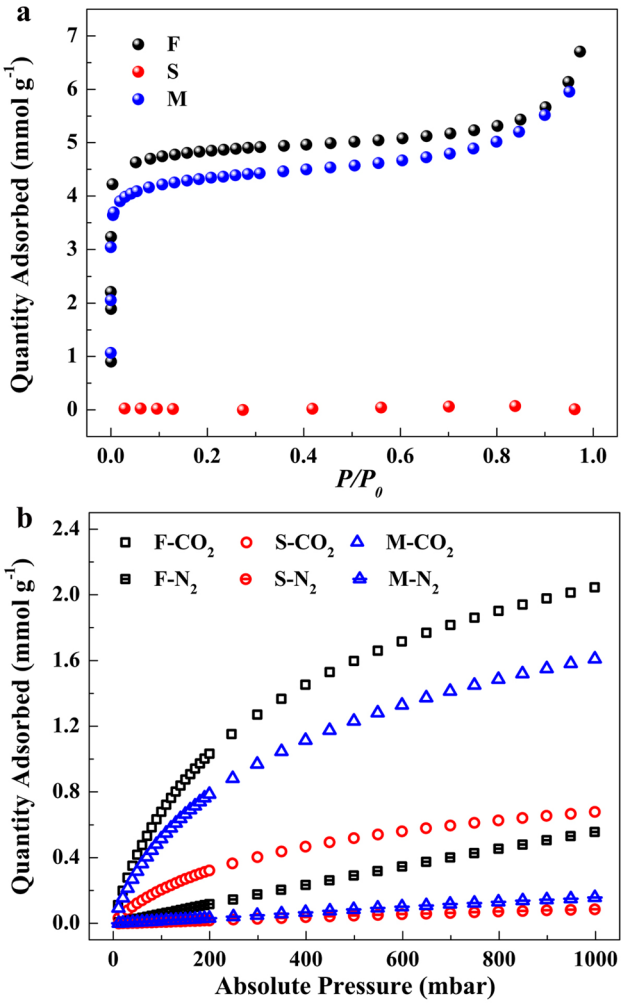

Figure 4. Single-component gas adsorption behaviors of MIP-203s. (a) N_2 adsorption isotherms collected at 77 K. (b) CO_2 and N_2 adsorption isotherms collected at 298 K.

by 58%, from 1.61 mmol g^{-1} at 273 K to 0.68 mmol g^{-1} at 298 K. In the case of MIP-203-F, only a 24% reduction (2.72 to 2.05 mmol g^{-1}) in CO_2 uptake at 1 bar was observed from 273 to 298 K. Therefore, MIP-203-F and MIP-203-S indeed display huge differences in their structural responses to gaseous guest molecules, as expected. MIP-203-M behaves more similarly to MIP-203-F than MIP-203-S, likely due to the higher composition of fumarate linker in its structural framework.

To check the structural response of the MOF framework in the presence of CO_2 guest molecules, *in situ* PXRD data along the adsorption of CO_2 under various pressures was collected on the three MIP-203 samples at room temperature. As shown in Figure 5, both activated MIP-203-F and MIP-203-M structures could easily swell back to the open form under a low CO_2 pressure (between 200 and 300 mbar), highlighting their swelling flexibility. Further increasing the CO_2 pressure did not have any notable effects on the samples' structural expansion. However, the activated MIP-203-S sample remained in its closely packed configuration throughout the entire range of CO_2 pressures applied. Even high CO_2 pressure (6 bar) was not able to reopen the framework, which is consistent with its lower CO_2 uptake compared to those of MIP-203-F and MIP-203-M under the same condition.

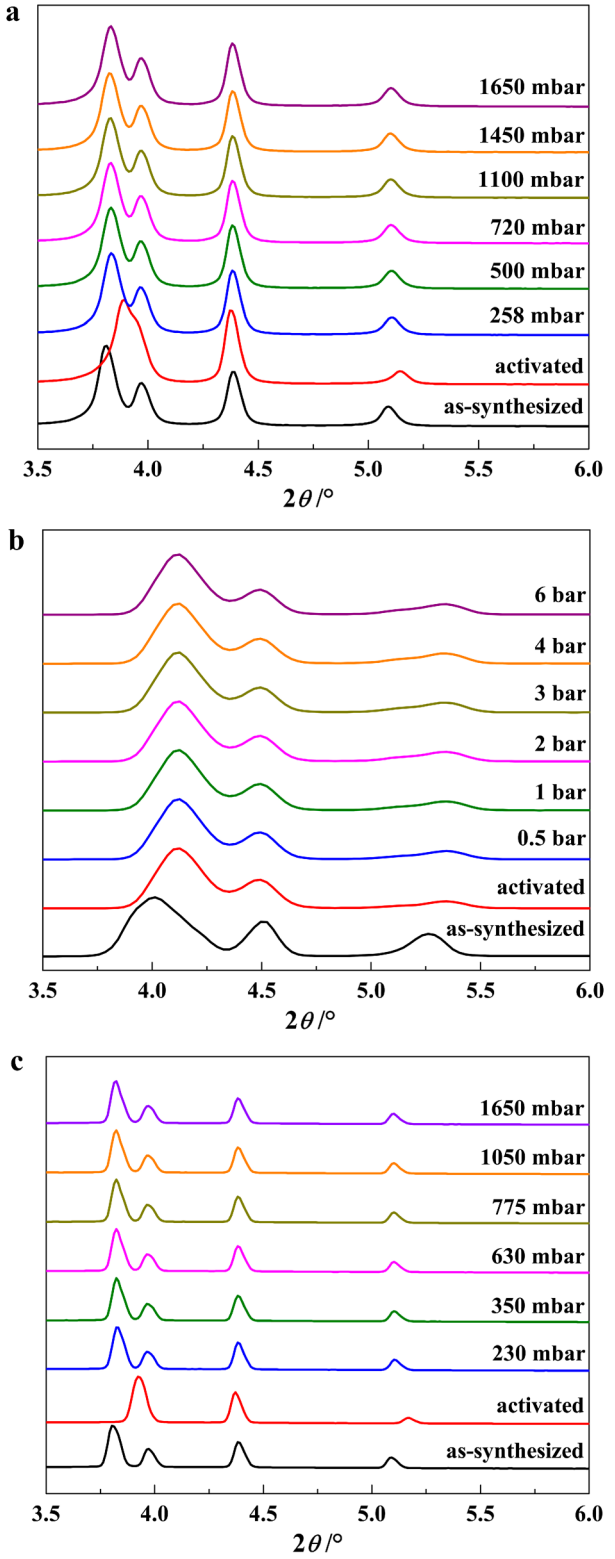

Figure 5. *In situ* PXRD patterns of MIP-203s along adsorption of CO_2 under different pressures at room temperature. (a) MIP-203-F. (b) MIP-203-S. (c) MIP-203-M.

To evaluate the adsorption affinity, isosteric heats of adsorption (Q_{st}) were calculated with the CO_2 adsorption isotherms at 273, 298, and 303 K in the pressure range of 0−1 bar. At zero coverage, the Q_{st} values are 32, 34, and 33 kJ mol^{-1} for MIP-203-F, MIP-203-S, and MIP-203-M, respectively. The

DOI: 10.1021/jacs.9b07816
J. Am. Chem. Soc. 2019, 141, 17207−17216

working capacities of CO_2 sorption (Wc(1−0.1 bar)) for three MIP-203 samples were calculated to be 1.38, 1.04, and 1.15 mmol/g for MIP-203-F, MIP-203-S, and MIP-203-M, respectively, at 273 K. The corresponding values at 298 K are 1.35, 0.47, and 1.09 mmol/g. It is interesting to note that the working capacities for both the MIP-203-F and MIP-203-M compounds showed far less dependence on the working temperature, while the working capacity of MIP-203-S exhibited dramatic sensitivity toward the applied temperature, decreasing by more than half when the testing temperature increased from 273 to 298 K. Furthermore, ideal adsorbed solution theory (IAST)[52,53] was applied to evaluate the adsorption selectivity of CO_2/N_2 for MIP-203s when a binary gaseous mixture of CO_2/N_2 = 15:85 (v:v) at 298 K was considered (Figure S14). The corresponding selectivities were calculated to be 15, 34, and 51 for MIP-203-F, MIP-203-S, and MIP-203-M, respectively (Figure S14), which are in the usual range for MOF-based CO_2 adsorbents.[54,55]

It is worth noting that MIP-203-S shows a selectivity twice as high as that of MIP-203-F, highlighting the linker softness effect that interferes with nitrogen entering the pores. However, MIP-203-M outperforms MIP-203-S in terms of selectivity by a margin of 50%. The above comparison of the working capacity and adsorptive selectivity between the three MIP-203 compounds suggests that the introduction of proper local softness into a structurally flexible MOF framework would result in a favorable combination of accessible porosity and structural dynamics, leading to an optimal balance for selective CO_2 separation in terms of working capacity and selectivity.

CONCLUSION

In summary, we report a series of flexible isostructural Zr-MOFs synthesized on the basis of natural C4 linkers (MIP-203s), in which the structural dynamics can be engineered on the basis of the differences in freedom of linker bond stretching and rotation between rigid fumarate and soft succinate. Comprehensive characterizations of structural responses to diverse external stimuli, including thermal changes as well as liquid and gaseous guest molecules, have been conducted to correlate the corresponding linker's flexibility with MOF dynamics. Directed by this established correlation, MIP-203-M, with a proper multivariate flexibility that efficiently combines swelling and linker distortion or bending, was evaluated for the adsorptive separation of CO_2/N_2. It not only exhibits a good working capacity for CO_2 adsorption under the working condition benefiting from the swelling MIP-203-F framework but also has a significantly enhanced selectivity for CO_2/N_2 compared with those of the MIP-203-F and -S forms, owing to the linker stretching and rotational flexibility generated from the soft succinate skeleton. In principle, this strategy could be applied to the separation of other chemical mixtures, including liquid and gaseous phases. Therefore, it serves as a suitable example that engineering the structural flexibility of MOF materials could constitute a promising and versatile strategy for improving MOF separation performance, or even realizing new applications.

ASSOCIATED CONTENT

Supporting Information

The Supporting Information is available free of charge on the ACS Publications website at DOI: 10.1021/jacs.9b07816.

Vibration modes (MP4)

Vibration modes (MP4)

CIF data (CIF)

checkCIF/PLATON report (PDF)

Materials and instruments, details of syntheses, crystal structure determination, tables of structural parameters, torsion angles, unit cell parameters, MOFs phonon modes, and virial equation parameters, figures of powder diffraction patterns, PSD, cluster geometries, potential energy profile, NMR, IR, and Raman spectra, thermal stability plots, PXRD patterns, adsorption isotherms, and Q_{st} vs loading, computational details, and IAST calculations (PDF)

AUTHOR INFORMATION

Corresponding Authors

*E-mail: kuitan@utdallas.edu.

*E-mail: guillaume.maurin1@umontpellier.fr.

*E-mail: christian.serre@ens.fr.

ORCID

Sujing Wang: 0000-0003-0942-2907

Kolade Oyekan: 0000-0003-1394-4548

William Shepard: 0000-0002-5724-1193

Charlotte Martineau-Corcos: 0000-0003-1887-1042

Yaroslav Filinchuk: 0000-0002-6146-3696

Kui Tan: 0000-0002-5167-7295

Christian Serre: 0000-0003-3040-2564

Notes

The authors declare no competing financial interest.

ACKNOWLEDGMENTS

The authors from France are grateful to the ANR Project MeaCoPA (ANR-17-CE29-0003) for financial support. The spectroscopic characterization and analysis (IR and Raman) were supported by the US Department of Energy, Office of Science, Office of Basic Energy Sciences; it started under Award No. DE-FG02-08ER46491 and finished under Award No. DE-SC0019902.

REFERENCES

(1) Kitagawa, S.; Kondo, M. Functional micropore chemistry of crystalline metal complex-assembled compounds. *Bull. Chem. Soc. Jpn.* **1998**, *71* (8), 1739−1753.

(2) Bureekaew, S.; Shimomura, S.; Kitagawa, S. Chemistry and application of flexible porous coordination polymers*. *Sci. Technol. Adv. Mater.* **2008**, *9* (1), 014108.

(3) Liu, J.; Chen, L.; Cui, H.; Zhang, J.; Zhang, L.; Su, C. Y. Applications of metal-organic frameworks in heterogeneous supramolecular catalysis. *Chem. Soc. Rev.* **2014**, *43* (16), 6011−61.

(4) Horike, S.; Shimomura, S.; Kitagawa, S. Soft porous crystals. *Nat. Chem.* **2009**, *1* (9), 695−704.

(5) Kitagawa, S.; Kitaura, R.; Noro, S. Functional porous coordination polymers. *Angew. Chem., Int. Ed.* **2004**, *43* (18), 2334−75.

(6) Seo, J.; Matsuda, R.; Sakamoto, H.; Bonneau, C.; Kitagawa, S. A pillared-layer coordination polymer with a rotatable pillar acting as a molecular gate for guest molecules. *J. Am. Chem. Soc.* **2009**, *131* (35), 12792−800.

(7) Loiseau, T.; Serre, C.; Huguenard, C.; Fink, G.; Taulelle, F.; Henry, M.; Bataille, T.; Férey, G. A Rationale for the Large Breathing of the Porous Aluminum Terephthalate (MIL-53) Upon Hydration. *Chem. - Eur. J.* **2004**, *10* (6), 1373−1382.

DOI: 10.1021/jacs.9b07816
J. Am. Chem. Soc. 2019, 141, 17207−17216

(8) Mellot-Draznieks, C.; Serre, C.; Surble, S.; Audebrand, N.; Ferey, G. Very large swelling in hybrid frameworks: a combined computational and powder diffraction study. *J. Am. Chem. Soc.* **2005**, *127* (46), 16273−8.
(9) Krause, S.; Bon, V.; Stoeck, U.; Senkovska, I.; Tobbens, D. M.; Wallacher, D.; Kaskel, S. A Stimuli-Responsive Zirconium Metal-Organic Framework Based on Supermolecular Design. *Angew. Chem., Int. Ed.* **2017**, *56* (36), 10676−10680.
(10) Qin, J. S.; Yuan, S.; Alsalme, A.; Zhou, H. C. Flexible Zirconium MOF as the Crystalline Sponge for Coordinative Alignment of Dicarboxylates. *ACS Appl. Mater. Interfaces* **2017**, *9* (39), 33408−33412.
(11) Zhang, Y.; Zhang, X.; Lyu, J.; Otake, K. I.; Wang, X.; Redfern, L. R.; Malliakas, C. D.; Li, Z.; Islamoglu, T.; Wang, B.; Farha, O. K. A Flexible Metal-Organic Framework with 4-Connected Zr6 Nodes. *J. Am. Chem. Soc.* **2018**, *140* (36), 11179−11183.
(12) Brown, J. W.; Henderson, B. L.; Kiesz, M. D.; Whalley, A. C.; Morris, W.; Grunder, S.; Deng, H. X.; Furukawa, H.; Zink, J. I.; Stoddart, J. F.; Yaghi, O. M. Photophysical pore control in an azobenzene-containing metal-organic framework. *Chem. Sci.* **2013**, *4* (7), 2858−2864.
(13) Modrow, A.; Zargarani, D.; Herges, R.; Stock, N. The first porous MOF with photoswitchable linker molecules. *Dalton Trans* **2011**, *40* (16), 4217−22.
(14) Liu, Y.; Her, J. H.; Dailly, A.; Ramirez-Cuesta, A. J.; Neumann, D. A.; Brown, C. M. Reversible structural transition in MIL-53 with large temperature hysteresis. *J. Am. Chem. Soc.* **2008**, *130* (35), 11813−8.
(15) DeVries, L. D.; Barron, P. M.; Hurley, E. P.; Hu, C.; Choe, W. "Nanoscale lattice fence" in a metal-organic framework: interplay between hinged topology and highly anisotropic thermal response. *J. Am. Chem. Soc.* **2011**, *133* (38), 14848−51.
(16) Henke, S.; Schneemann, A.; Fischer, R. A. Massive Anisotropic Thermal Expansion and Thermo-Responsive Breathing in Metal-Organic Frameworks Modulated by Linker Functionalization. *Adv. Funct. Mater.* **2013**, *23* (48), 5990−5996.
(17) Ghoufi, A.; Benhamed, K.; Boukli-Hacene, L.; Maurin, G. Electrically Induced Breathing of the MIL-53(Cr) Metal-Organic Framework. *ACS Cent. Sci.* **2017**, *3* (5), 394−398.
(18) Chapman, K. W.; Halder, G. J.; Chupas, P. J. Pressure-induced amorphization and porosity modification in a metal-organic framework. *J. Am. Chem. Soc.* **2009**, *131* (48), 17546−7.
(19) Gagnon, K. J.; Beavers, C. M.; Clearfield, A. MOFs under pressure: the reversible compression of a single crystal. *J. Am. Chem. Soc.* **2013**, *135* (4), 1252−5.
(20) Goodwin, A. L.; Keen, D. A.; Tucker, M. G. Large negative linear compressibility of Ag3[Co(CN)6]. *Proc. Natl. Acad. Sci. U. S. A.* **2008**, *105* (48), 18708−13.
(21) Yot, P. G.; Ma, Q.; Haines, J.; Yang, Q.; Ghoufi, A.; Devic, T.; Serre, C.; Dmitriev, V.; Férey, G.; Zhong, C.; Maurin, G. Large breathing of the MOF MIL-47(VIV) under mechanical pressure: a joint experimental−modelling exploration. *Chem. Sci.* **2012**, *3* (4), 1100−1104.
(22) Schneemann, A.; Bon, V.; Schwedler, I.; Senkovska, I.; Kaskel, S.; Fischer, R. A. Flexible metal−organic frameworks. *Chem. Soc. Rev.* **2014**, *43* (16), 6062−6096.
(23) Lin, Z. J.; Lu, J.; Hong, M.; Cao, R. Metal-organic frameworks based on flexible ligands (FL-MOFs): structures and applications. *Chem. Soc. Rev.* **2014**, *43* (16), 5867−95.
(24) Férey, G. Giant flexibility of crystallized organic−inorganic porous solids: facts, reasons, effects and applications. *New J. Chem.* **2016**, *40* (5), 3950−3967.
(25) Férey, G. Structural flexibility in crystallized matter: from history to applications. *Dalton Trans.* **2016**, *45* (10), 4073−4089.
(26) Bousquet, D.; Coudert, F. X.; Fossati, A. G.; Neimark, A. V.; Fuchs, A. H.; Boutin, A. Adsorption induced transitions in soft porous crystals: an osmotic potential approach to multistability and intermediate structures. *J. Chem. Phys.* **2013**, *138* (17), 174706.
(27) Coudert, F.-X.; Boutin, A.; Fuchs, A. H.; Neimark, A. V. Adsorption Deformation and Structural Transitions in Metal−Organic Frameworks: From the Unit Cell to the Crystal. *J. Phys. Chem. Lett.* **2013**, *4* (19), 3198−3205.
(28) Schneemann, A.; Bon, V.; Schwedler, I.; Senkovska, I.; Kaskel, S.; Fischer, R. A. Flexible metal−organic frameworks. *Chem. Soc. Rev.* **2014**, *43* (16), 6062−6096.
(29) Krause, S.; Bon, V.; Senkovska, I.; Stoeck, U.; Wallacher, D.; Többens, D. M.; Zander, S.; Pillai, R. S.; Maurin, G.; Coudert, F.-X.; Kaskel, S. A pressure-amplifying framework material with negative gas adsorption transitions. *Nature* **2016**, *532*, 348.
(30) Férey, G.; Serre, C. Large breathing effects in three-dimensional porous hybrid matter: facts, analyses, rules and consequences. *Chem. Soc. Rev.* **2009**, *38* (5), 1380−1399.
(31) Katsoulidis, A. P.; Antypov, D.; Whitehead, G. F. S.; Carrington, E. J.; Adams, D. J.; Berry, N. G.; Darling, G. R.; Dyer, M. S.; Rosseinsky, M. J. Chemical control of structure and guest uptake by a conformationally mobile porous material. *Nature* **2019**, *565* (7738), 213−217.
(32) Bueken, B.; Vermoortele, F.; Vanpoucke, D. E.; Reinsch, H.; Tsou, C. C.; Valvekens, P.; De Baerdemaeker, T.; Ameloot, R.; Kirschhock, C. E.; Van Speybroeck, V.; Mayer, J. M.; De Vos, D. A Flexible Photoactive Titanium Metal-Organic Framework Based on a [Ti(IV)3(mu3-O)(O)2(COO)6] Cluster. *Angew. Chem., Int. Ed.* **2015**, *54* (47), 13912−7.
(33) Bueken, B.; Vermoortele, F.; Cliffe, M. J.; Wharmby, M. T.; Foucher, D.; Wieme, J.; Vanduyfhuys, L.; Martineau, C.; Stock, N.; Taulelle, F.; Van Speybroeck, V.; Goodwin, A. L.; De Vos, D. A Breathing Zirconium Metal−Organic Framework with Reversible Loss of Crystallinity by Correlated Nanodomain Formation. *Chem. - Eur. J.* **2016**, *22* (10), 3264−3267.
(34) Bai, Y.; Dou, Y.; Xie, L. H.; Rutledge, W.; Li, J. R.; Zhou, H. C. Zr-based metal-organic frameworks: design, synthesis, structure, and applications. *Chem. Soc. Rev.* **2016**, *45* (8), 2327−67.
(35) Gu, C.; Hosono, N.; Zheng, J. J.; Sato, Y.; Kusaka, S.; Sakaki, S.; Kitagawa, S. Design and control of gas diffusion process in a nanoporous soft crystal. *Science* **2019**, *363* (6425), 387−391.
(36) Furukawa, H.; Gandara, F.; Zhang, Y. B.; Jiang, J.; Queen, W. L.; Hudson, M. R.; Yaghi, O. M. Water adsorption in porous metal-organic frameworks and related materials. *J. Am. Chem. Soc.* **2014**, *136* (11), 4369−81.
(37) SK, M.; Bhowal, S.; Biswas, S. Synthesis, Characterization, Stability, and Gas Adsorption Characteristics of a Highly Stable Zirconium Mesaconate Framework Material. *Eur. J. Inorg. Chem.* **2015**, *2015* (20), 3317−3322.
(38) Wang, S.; Wahiduzzaman, M.; Martineau-Corcos, C.; Maurin, G.; Serre, C. A Microporous Zirconium Metal-Organic Framework Based on Trans-aconitic Acid for Selective Carbon Dioxide Adsorption. *Eur. J. Inorg. Chem.* **2019**, *2019* (22), 2674−2679.
(39) Wang, S.; Wahiduzzaman, M.; Davis, L.; Tissot, A.; Shepard, W.; Marrot, J.; Martineau-Corcos, C.; Hamdane, D.; Maurin, G.; Devautour-Vinot, S.; Serre, C. A robust zirconium amino acid metal-organic framework for proton conduction. *Nat. Commun.* **2018**, *9* (1), 4937.
(40) Alvarez, E.; Guillou, N.; Martineau, C.; Bueken, B.; Van de Voorde, B.; Le Guillouzer, C.; Fabry, P.; Nouar, F.; Taulelle, F.; de Vos, D.; Chang, J.-S.; Cho, K. H.; Ramsahye, N.; Devic, T.; Daturi, M.; Maurin, G.; Serre, C. The Structure of the Aluminum Fumarate Metal−Organic Framework A520. *Angew. Chem., Int. Ed.* **2015**, *54* (12), 3664−3668.
(41) Livage, C.; Egger, C.; Nogues, M.; Ferey, G. Hybrid open frameworks (MIL-n). Part 5 - Synthesis and crystal structure of MIL-9: a new three-dimensional ferrimagnetic cobalt(II) carboxylate with a two-dimensional array of edge-sharing Co octahedra with 12-membered rings. *J. Mater. Chem.* **1998**, *8* (12), 2743−2747.
(42) Livage, C.; Egger, C.; Férey, G. Hybrid Open Networks (MIL 16): Synthesis, Crystal Structure, and Ferrimagnetism of Co4(OH)-2(H2O)2(C4H4O4)3·2H2O, a New Layered Cobalt(II) Carboxylate

DOI: 10.1021/jacs.9b07816
J. Am. Chem. Soc. 2019, 141, 17207−17216

with 14-Membered Ring Channels. *Chem. Mater.* **1999**, *11* (6), 1546−1550.
(43) Wißmann, G.; Schaate, A.; Lilienthal, S.; Bremer, I.; Schneider, A. M.; Behrens, P. Modulated synthesis of Zr-fumarate MOF. *Microporous Mesoporous Mater.* **2012**, *152*, 64−70.
(44) Wang, S.; Kitao, T.; Guillou, N.; Wahiduzzaman, M.; Martineau-Corcos, C.; Nouar, F.; Tissot, A.; Binet, L.; Ramsahye, N.; Devautour-Vinot, S.; Kitagawa, S.; Seki, S.; Tsutsui, Y.; Briois, V.; Steunou, N.; Maurin, G.; Uemura, T.; Serre, C. A phase transformable ultrastable titanium-carboxylate framework for photoconduction. *Nat. Commun.* **2018**, *9* (1), 1660.
(45) Wahiduzzaman, M.; Wang, S.; Sikora, B. J.; Serre, C.; Maurin, G. Computational structure determination of novel metal-organic frameworks. *Chem. Commun.* **2018**, *54* (77), 10812−10815.
(46) Duran, D.; Couster, S. L.; Desjardins, K.; Delmotte, A.; Fox, G.; Meijers, R.; Moreno, T.; Savko, M.; Shepard, W. PROXIMA 2A − A New Fully Tunable Micro-focus Beamline for Macromolecular Crystallography. *J. Phys.: Conf. Ser.* **2013**, *425* (1), 012005.
(47) Cavka, J. H.; Jakobsen, S.; Olsbye, U.; Guillou, N.; Lamberti, C.; Bordiga, S.; Lillerud, K. P. A new zirconium inorganic building brick forming metal organic frameworks with exceptional stability. *J. Am. Chem. Soc.* **2008**, *130* (42), 13850−1.
(48) Nijem, N.; Wu, H.; Canepa, P.; Marti, A.; Balkus, K. J., Jr.; Thonhauser, T.; Li, J.; Chabal, Y. J. Tuning the gate opening pressure of Metal-Organic Frameworks (MOFs) for the selective separation of hydrocarbons. *J. Am. Chem. Soc.* **2012**, *134* (37), 15201−4.
(49) Sato, H.; Kosaka, W.; Matsuda, R.; Hori, A.; Hijikata, Y.; Belosludov, R. V.; Sakaki, S.; Takata, M.; Kitagawa, S. Self-accelerating CO sorption in a soft nanoporous crystal. *Science* **2014**, *343* (6167), 167−70.
(50) Shimomura, S.; Higuchi, M.; Matsuda, R.; Yoneda, K.; Hijikata, Y.; Kubota, Y.; Mita, Y.; Kim, J.; Takata, M.; Kitagawa, S. Selective sorption of oxygen and nitric oxide by an electron-donating flexible porous coordination polymer. *Nat. Chem.* **2010**, *2* (8), 633−7.
(51) Maji, T. K.; Matsuda, R.; Kitagawa, S. A flexible interpenetrating coordination framework with a bimodal porous functionality. *Nat. Mater.* **2007**, *6* (2), 142−8.
(52) Bae, Y. S.; Farha, O. K.; Spokoyny, A. M.; Mirkin, C. A.; Hupp, J. T.; Snurr, R. Q. Carborane-based metal-organic frameworks as highly selective sorbents for CO(2) over methane. *Chem. Commun.* **2008**, No. 35, 4135−7.
(53) Heuchel, M.; Snurr, R. Q.; Buss, E. Adsorption of CH4−CF4Mixtures in Silicalite: Simulation, Experiment, and Theory. *Langmuir* **1997**, *13* (25), 6795−6804.
(54) Benoit, V.; Pillai, R. S.; Orsi, A.; Normand, P.; Jobic, H.; Nouar, F.; Billemont, P.; Bloch, E.; Bourrelly, S.; Devic, T.; Wright, P. A.; de Weireld, G.; Serre, C.; Maurin, G.; Llewellyn, P. L. MIL-91(Ti), a small pore metal−organic framework which fulfils several criteria: an upscaled green synthesis, excellent water stability, high CO2 selectivity and fast CO2 transport. *J. Mater. Chem. A* **2016**, *4* (4), 1383−1389.
(55) Liu, J.; Thallapally, P. K.; McGrail, B. P.; Brown, D. R.; Liu, J. Progress in adsorption-based CO2 capture by metal-organic frameworks. *Chem. Soc. Rev.* **2012**, *41* (6), 2308−22.

DOI: 10.1021/jacs.9b07816
J. Am. Chem. Soc. 2019, 141, 17207−17216